Label-Free SnO_2 Nanowire FET Biosensor for Protein Detection

Label-Free SnO_2 Nanowire FET Biosensor for Protein Detection

Markus H. Jakob[a*], Bo Dong[a], Sebastian Gutsch[a], Claire Chatelle[b], Abinaya Krishnaraja[a], Wilfried Weber[b] and Margit Zacharias[a]

[a]Laboratory for Nanotechnology, Department of Microsystems Engineering – IMTEK, University of Freiburg, Georges-Koehler-Allee 103, 79110 Freiburg im Breisgau, Germany.

[b]Faculty of Biology, Centre for Biological Signalling Studies (BIOSS), University of Freiburg, Schänzlestrasse 1, 79104 Freiburg, Germany.

*Corresponding author: E-mail address: markus.jakob@imtek.uni-freiburg.de

ABSTRACT

Novel tin oxide field-effect-transistors (SnO_2 NW-FET) for pH and protein detection applicable in the healthcare sector are reported. With the presented SnO_2 NW-FET the proof-of-concept of a bio-sensing device is demonstrated using the carrier transport control of the FET channel by a (bio-) liquid modulated gate. Ultra-thin Al_2O_3 fabricated by a low temperature atomic layer deposition (ALD) process represents a sensitive layer to H^+ ions safeguarding the nanowire at the same time. Successful pH sensitivity is demonstrated for pH ranging from 3 to 10. For protein detection, the SnO_2 NW-FET is functionalized with a receptor molecule which specifically interacts with the protein of interest to be detected. The feasibility of this approach is demonstrated via the detection of a biotinylated protein using a NW-FET functionalized with streptavidin. An immediate label-free electronic read-out of the signal is shown. The well-established Enzyme-Linked Immunosorbent Assay (ELISA) method is used to determine the optimal experimental procedure which would enable molecular binding events to happen while being compatible with a final label-free electronic read-out on a NW-FET. Integration of the bottom-up fabricated SnO_2 NW-FET pH- and biosensor into a microfluidic system (lab-on-a-chip) allows the automated analysis of small volumes in the 400 µl range as would be desired in portable on-site point-of-care (POC) devices for medical diagnosis.

KEYWORDS

nanowire (NW), field-effect-transistor (FET), biosensor, bottom-up, label-free, biomolecule, real-time

INTRODUCTION

With the increasing demand for point-of-care (POC) devices in the healthcare sector, the research in the field of biosensors based on field-effect-transistors (FET) has grown dramatically over the last couple of years. Especially one-dimensional (1-D) structures such as nanowires, nanotubes, nanobelts and nanorods are promising candidates due to their high sensitivity. Hereby, silicon nanowires represent by far the most investigated nanostructures [1–7]. Apart from silicon, metal-oxide semiconductor (MOS) devices such as ZnO, SnO_2, In_2O_3 or TiO_2 are possible alternatives for real-time and label-free detection of charged biomolecules (e.g. proteins, nucleic acids, cells, viruses [8]) with zinc oxide (ZnO) being the most popular one [9–13]. So far, tin oxide (SnO_2) nanowires have been widely explored only as gas sensors [14,15].

In this paper we demonstrate the use of a novel SnO_2 NW-FET to use as a pH- and biosensor. The specific detection of a protein with such a sensor is realized by using the field-effect. Common sensors are based on CMOS technology, but we think that using SnO_2 nanowires may offer significant advantages. Firstly, our here used SnO_2 nanowires possess an intrinsic n-type doping and thus avoid the need for intentional doping. Oxygen vacancies are responsible for the n-type semiconductor behavior without doping [14]. It is well known, for silicon nanowires, that surface segregation of dopants and dielectric screening cause serious challenges to achieve reliable doping [16]. Secondly, SnO_2 nanowires exhibit high crystallinity with a wide band gap of 3.6 eV [17]. Thus, its transparency in the visible range allows the use of SnO_2 devices without complex packaging. A further advantage of our sensor is the chemical robustness, e.g. physiological solutions (pH 3 to 10), of the SnO_2 nanowires [18].

In a typical FET, a voltage is applied to the insulated metal top gate to regulate the current of the underlying semiconductor. For an n-type semiconductor applying a positive gate voltage results in an attraction of negative charge carriers in the drain-source-channel and thus in an increase in current. In contrast, a negative gate voltage results in a decrease in drain-source current due to repulsion of negative charge carriers within the channel. To transfer these concepts to pH- and biosensors the metal top gate has to be replaced by an investigated electrolyte solution. Instead of applying an external voltage, the drain-source current can then be directly modulated by the electrolyte pH or by the adsorption of the intrinsically charged biomolecules within the electrolyte solution on the transistor gate oxide. For pH sensors the proton (H^+) ion concentration is measured resulting in a change of the net surface charge of the gate oxide [19]. Using an additional insulating Al_2O_3 shell layer offers a specific number of OH hydroxyl groups which can be protonated/deprotonated (site-binding model) by H^+ in the electrolyte solution [20–22]. In general the respective oxide surface can appear as Al-O^-, Al-OH^{2+} and Al-OH [23]. As a result the drain-source current through the nanowire will be modulated.

In case of a specific protein detection, the sensor surface has to be additionally functionalized with a receptor biomolecule. The intrinsically charged protein of interest binds to its receptor in close distance to the sensor surface. The electric field of the protein causes, just like the external applied voltage in the typical FET, an attraction (accumulation) or repulsion (depletion) of negative charge carriers (n-type semiconductor) for a positively or negatively charged molecule respectively [8]. Hence, the drain-source current changes. In this work, we used the streptavidin-biotin pair, which has one of the strongest noncovalent binding characteristics known [24–27], to demonstrate the applicability of the sensor for protein detection. The sensor surface, functionalized with streptavidin, should enable the detection of

any biotinylated protein of interest, here the tetracycline repressor bTetR. The well-established Enzyme-linked immunosorbent assay (ELISA) technology, can be used to determine the optimal assay procedure and to verify the obtained results. ELISAs are based on the same binding mechanism but require an additional detection element to translate the molecular binding event into a detectable signal. For optical read-out, the detection element is often an antibody coupled to an enzyme which catalyzes the formation of a colorful product. The enzymatic reaction can be optically followed and reflects the quantity of protein of interest present in the sample.

There are two modes of fabrication for single NW-FET devices. For silicon both the top-down and the bottom-up approach are used rather frequently [2]. However, fabricating metal-oxide nanowires usually necessitates the latter [10]. Metal-oxide nanowires are typically prepared by vapor-solid (VS) or vapor-liquid-solid (VLS) growth. This vapor phase transport technique allows fast fabrication of countless nanowires but at the same time faces difficulties in contacting selected single nanowires. In contrast to the top-down method, nanowires are not located on a precise positions but have to be found and contacted individually [28]. However, using guided growth of nanowires could help bypass this challenge of unspecified nanowire location on substrates and help to ease the fabrication processes in the future [29,30].

A microfluidic cell is normally used to establish a liquid gate. Here, a polydimethylsiloxane (PDMS) channel is prepared where small volumes down to the range of 400 µl can easily be examined in an automatic and precise way. Integral part of the here used measurement setup is a flow-thru 3 M KCl Silver/Silver Chloride (Ag/AgCl) reference electrode. A reference electrode is indispensable to receive reliable and reproducible results. Its main task is the indemnification of a constant electrostatic potential during the measurement independent of the

used electrolyte solution [31,32]. Without having a well-defined solution potential a change of current is meaningless [33]. Furthermore the reference electrode is used to set the solution potential to the optimal, most sensitive measurement regime of the SnO_2 NW-FET pH- and biosensor.

EXPERIMENTAL

SnO_2 nanowire growth

N-type SnO_2 nanowires were grown by an Au catalyzed thermal chemical vapor deposition (CVD) process in a one-zone heating furnace (Fig. 1a). The SnO_2 nanowires were synthesized on a silicon substrate with an evaporated 2 nm thin Au layer serving as the catalyst for the vapor-liquid-solid (VLS) process. SnO_2 (9 %, Sigma-Aldrich) powder and a graphite powder (99.9995 %, Alfa Aesar) were mixed together in a 1:1 mass ratio. One gram of the mixture was transferred into a quartz boat and placed in the middle of the heating furnace. The substrate was placed before the source on the gas inlet side. In this case, the nanowires grew upstream. After pumping down to $p < 0.1$ mbar in the tube, a constant gas flow consisting of Ar carrier gas (20 sccm) and an O_2 gas (1 sccm) was initiated as pre-flow process. Reaching the desired pressure of 200 mbar the heating process was started. The heating zone was set to T = 950 °C for a growth time of 30 min [34,35]. The Au dot seen in Fig. 1b indicates the VLS growths mechanism. Fig. 1c shows an SEM image of a typical as-grown VLS square SnO_2 nanowires with a size between 100 nm and 150 nm.

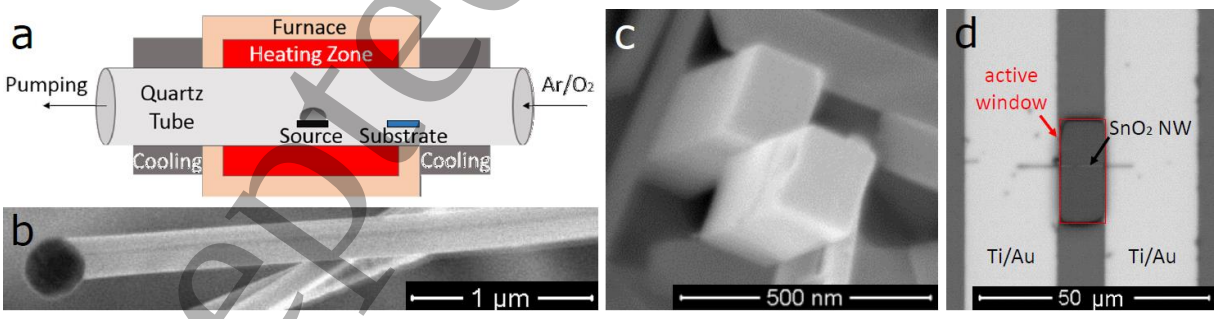

Figure 1. (a) Schematic diagram of a one-zone CVD furnace setup for Au catalyzed SnO_2 nanowire synthesis in upstream mode. SEM image of one as-grown vapor-liquid-solid (VLS) square SnO_2 nanowire (b) with Au dot on top indicating a VLS growths mechanism (c) and two broken individual SnO_2 nanowires showing their cross section with its square profile. (d)

Optical image of a SnO_2 NW-FET pH sensor (biosensor). The red rectangle highlights the active window (8 μm × 20 μm) where the electrolyte solution is in direct contact with the Al_2O_3-coated SnO_2 NW.

Device Fabrication

The substrates used here for SnO_2 NW-FET device fabrication were n-doped (1-30 Ohm-cm) 4-inch silicon (100) wafers where a 500 nm thick isolating silicon dioxide (SiO_2) layer was formed by wet oxidation at T = 950 °C. Theoretically, also other insulating substrates i.e. glass could be used [36,37]. The as-grown VLS SnO_2 nanowires were scratched from their original carrying substrate and suspended in isopropyl alcohol (IPA). A 5 s ultra-sonication step helped decomposing the nanowires within the solution before spin coating (800 rpm) the nanowire/IPA mixture onto the oxidized substrate. The nanowires were distributed homogeneously over the whole wafer surface and the IPA evaporated residue-free. To contact selected single nanowires, an image reversal resist (AZ 5214E) was spin coated and patterned using the laser writer μPG 101 from Heidelberg Instruments GmbH (Germany). 50 nm/30 nm of evaporated Ti/Au contacts ensured good ohmic contacts of the single SnO_2 nanowires. For the SnO_2 NW-FET with metal top gate a 20 nm aluminum oxide (Al_2O_3) layer was deposited as gate oxide by atomic layer deposition (ALD) at 100 °C using a standard trimethylaluminum/water process. The metal gate was formed by evaporating 200 nm of aluminum in a second lithography step.

For good and controlled working of the SnO_2 NW-FET suspended in chemical solution one has to encapsulate part of the device to avoid leakage currents between the source and drain contacts through the electrolyte solution [10]. Hence, our SnO_2 NW-FETs working as pH sensors were covered with a second image reversal resist working as encapsulation after contacting the single

nanowire. After resist patterning only a small active window (8 μm × 20 μm, cf. Fig. 1d) remained open to the electrolyte solution. In case of the SnO_2 NW-FET with metal top gate a thin 10 nm Al_2O_3 insulation and encapsulation layer was deposited on the SnO_2 nanowire. Additionally, this film operated as sensitive layer to H^+ ions which was necessary for pH measurement. The process on the 4-inch Si substrate allowed the integration of multiple devices (chip size: 20 mm × 20 mm). Every sensor was then wedge-wedge wire bonded onto a chip carrier. The chip carrier later on connected via a 20 pin card edge to a Keithley 2636 Source Meter (Keithley Instruments, Inc.) functioning as measurement unit.

Microfluidic Channel Fabrication

Starting point for the microfluidic channel fabrication was again a 4-inch silicon wafer. Negative photosensitive SU-8 3050 resist was spin coated and patterned with the inverted microchannel design. The thickness of the resist defined the height of the emerging microchannel. After development, poly dimethylsiloxane (PDMS) made from Sylgard 184 was doused in liquid state. After a two day curing process in vacuum, the PDMS could be removed from the mold. A hyperdomeric needle with an outer diameter of 1.6 mm was used to add an inlet/outlet into the PDMS. To ensure a good adhesion between the PDMS and the SnO_2 NW-FET pH- and biosensor the PDMS was cleaned in acetone using an ultrasonic bath and isopropanol, respectively. After drying with a nitrogen air gun, the PDMS channel was UV/ozone cleaned for 2 min. After the PDMS surface preparation, the PDMS channel was mounted on top of the NW-FET pH- and biosensor. To finish the measurement setup, two Teflon (PTFE) tubes (TECHLAB GmbH) with an inner diameter of 0.7 mm were inserted into the inlet and the outlet of the mounted PDMS channel. While the outlet was hereby connected to a high-precision syringe pump (neMESYS, CETONI GmbH) the inlet was connected to an exchangeable reservoir over a flow-thru reference electrode (Microelectrodes, Inc.). For each

electrolyte solution about 400 µl were pumped through the microfluidic channel (Fig. 3b). This volume is composed of the volume of the hose connecting the reservoir to the PDMS channel, the PDMS channel itself (< 1 µl), the hose connecting the PDMS channel with the flow-thru reference electrode (~ 20 µl) as well as the hose connecting the flow-thru reference electrode to the pump. This means that the actual volume needed to successfully operate the sensor is about 20 µl.

pH

For the pH measurement 8 electrolyte buffer solutions with pH values changing from 3 to 10 were investigated. The SnO_2 NW-FET pH sensor was given a 10 min waiting time to establish a baseline in the starting pH 3 electrolyte solution at room temperature. The current I_{ds} was measured in real-time. After 10 min the electrolyte solution within the microfluidic chamber was exchanged for a fresh pH 3 solution including a 5 min waiting time. In the following, the electrolyte solution within the microfluidic chamber was gradually exchanged from pH 3 to pH 10 in steps of 1. Solutions with pH 4, 7 and 9 were bought from Mettler-Toledo AG, Switzerland. pH 3, 5, 6, 8 and 10 were self-made based on 0.2 M solution of citric acid, acetic acid, potassium phosphate, tris, and glycin buffers respectively adjusted to the desired pH value with NaOH or HCl solutions.

ELISA

The wells of a high binding 96-well microtiter plate (Costar cat. no 3590) were coated with streptavidin at 4 µg/mL (100 µl/well) at 4°C overnight. The surface of the wells was then blocked with 1 % BSA (Sigma-Aldrich, 300 µl/well) for 1 h before applying the his-tagged bTetR protein diluted to 0; 50; 100; 500; 1,000; 60,000 ng/mL for an additional hour at room

temperature. Incubations with 100 µl/well of mouse anti-His antibodies (Novagen) followed by secondary anti-mouse antibodies coupled to the enzyme horseradish peroxidase (HRP) (Santa Cruz Biotechnology) were performed successively during 1 h at room temperature. Finally 100 µl of substrate solution (0.2 M acetic acid pH 4 + 375 µg/mL ABTS + 0.06 % H_2O_2) were added to each well. The enzymatic reaction was followed via the measurement of product formation by spectrophotometry at 405 nm for 30 minutes. Between each step of the process, 3 successive washing steps with 300 µl/well buffer were performed to remove any unbound proteins. Each incubation steps and washing steps were done in the indicated PBS buffer (1/ 0.1/0.01 × PBS).

Protein Detection

Before starting the measurements using the NW FETs in the microfluidic channels the tube and flow-thru reference electrode insides were blocked with 1 % BSA in 1 × PBS for 1 h at room temperature. In this way an adsorption of the later inserted biomolecules on non-utilizable surfaces can be prevented. After assembling the sensor chip into the microfluidic setup 400 µl of streptavidin at 10 µg/ml was drawn into the microfluidic cell onto the nanowire sensor surface by a high-precision micro-pump. A flow rate of 5 µl/s was used for all injections if not stated otherwise. After 1 h, the microfluidic channel was successively washed with 1 × PBS and 0.01 × PBS. Apart from diminishing the salt concentration within the microfluidic cell the washing step makes sure to flush away any unbound streptavidin biomolecules. 400 µl of 1 % BSA dissolved in 1 × PBS was then pulled through the device to passivate the sensor surface thus preventing non-specific binding of any following proteins. After 1 h a second washing step removed excessive BSA within the microfluidic cell. 400 µl bTetR with a working concentration of 600 µg/ml in 1 × PBS was finally drawn into the microfluidic cell to saturate the surface reaction followed by a last washing step.

RESULTS AND DISCUSSIONS

I. Electrical Characterization

Before using the NW FET device under extreme conditions like a fluidic channel one has to understand the device characteristics from a basic pristine point of view. Here, we first characterized SnO_2 nanowires fabricated as typical nanowire FET with a metal top gate electrode separated by an insulating oxide. The drain-source current as a function of the top gate voltage is shown in Fig. 2a with a respective device configuration in Fig. 2b. As for all other FETs, the here presented SnO_2 nanowire were coated with an insulating Al_2O_3 layer. The current-voltage ($I_{ds} - V_{ds}$) represents the output characteristics of a typical SnO_2 NW-FET in enhancement for high top gate voltages. This originates from the n-type behavior of the FET where an increase in top gate voltage leads to an increase in drain-source current. The semi-logarithmic plotted transfer curve indicates a high on/off ratio larger than 10^6. This is in good agreement with [38], where single-crystalline SnO_2 nanobelts showed a 10^6 switching ratio. In [37] the drain-source current of SnO_2 nanowires was controllable over almost five orders of magnitude thus confirming good electrical characteristics of our here grown and used nanowires. For comparison reasons we like to mention that bottom-up fabricated n-type high-performance Si NWFETs reported in [39] also showed an on/off ratio in the range of 10^6. Our SnO_2 NW-FET can be turned off completely at a top gate voltage of less than V_g = -1.5 V. The steepest point of the transfer curve, in linear scale (no graph shown), describes where an additional increase or decrease of the top gate potential has the biggest influence on the drain-source current, i.e. the transducer is most sensitive to small variations in gate potential. For pH and protein measurements the reference voltage bias has to be set to its most sensitive point. For this FET the most sensitive point would be at a top gate voltage between V_g = 0.5 V and V_g = 1 V. This allows maximizing the relative drain-source current change while changing the surface potential.

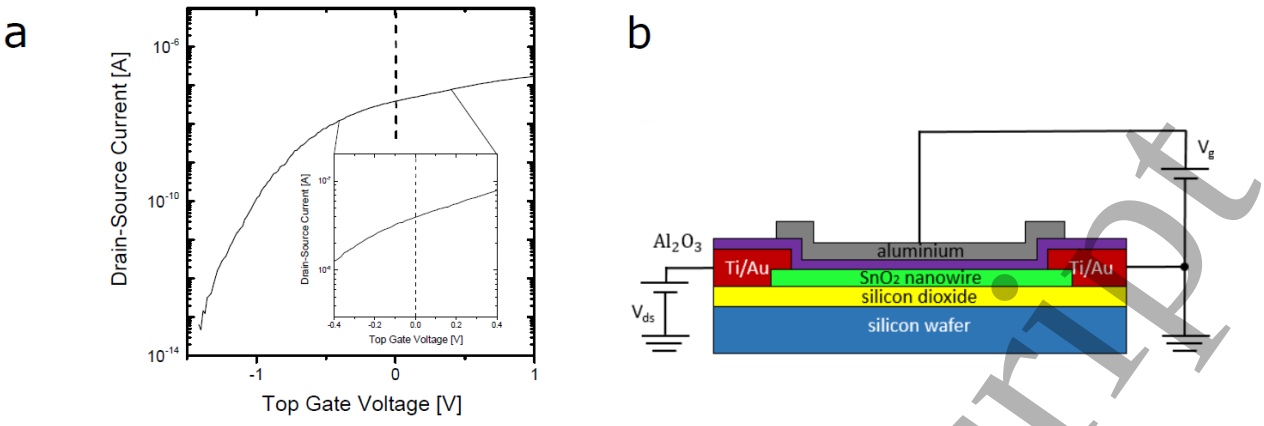

Figure 2. (a) Transfer (semi-logarithmic scale) characteristics (I_{ds} – V_{ref}) of a SnO_2 NW-FET with metal top gate at V_{ds} = 200 mV. Inset: Enlargement of the transfer characteristics from V_g = -0.4 V to V_g = 0.4 V. (b) Schematic side view diagram of a SnO_2 NW-FET with metal top gate.

II. pH Measurement

Now, the metal top gate is omitted to establish an oxide/electrolyte contact instead. For the SnO_2 NW-FET pH sensor the Al_2O_3 dielectric layer served as the H^+ ions sensitive film. The above already presented Fig. 1d shows the optical image of a single contacted SnO_2 nanowire. The active window (red rectangle) between the two contacts is free from the encapsulation resist to allow direct contact between the electrolyte solution and the Al_2O_3-coated SnO_2 nanowire.

To compare the metal top gate with a liquid gate we characterized a SnO_2 NW-FET pH sensor with a fluid gate using a reference solution (pH 3). An Ag/AgCl flow-thru reference electrode in contact with the solution was used to modulate the drain-source current by sweeping the reference voltage V_{ref} from 0 V to 2 V at a constant drain-source voltage V_{ds} = 100 mV. The drain-source current as a function of the liquid gate voltage (reference electrode) is shown in Fig. 3a with a respective device configuration in Fig. 3b. The drain-source current variation

(Fig. 3a) of the SnO_2 NW-FET pH sensor shows again a change of the current over 6 orders of magnitude and with that an on/off ratio larger than 10^6. Comparing it to the above presented typical FET (Fig. 2a) the pH sensor shows similar transfer characteristics. While both single-crystalline SnO_2 nanowires were fabricated simultaneously, differences in electrical characteristics can be explained by varying nanowire diameter. At a reference voltage of V_{ref} = 0 V the device is turned off completely. Applying a liquid gate potential caused a negative shift of the transfer curve by about V_{shift} = -1.2 V in comparison to a via metal top gate applied voltage. This shift can partially be explained by the different work functions of the metal used for the top gate (Al: ϕ = 4.1) and the reference electrode (Ag/AgCl: ϕ = 4.6).

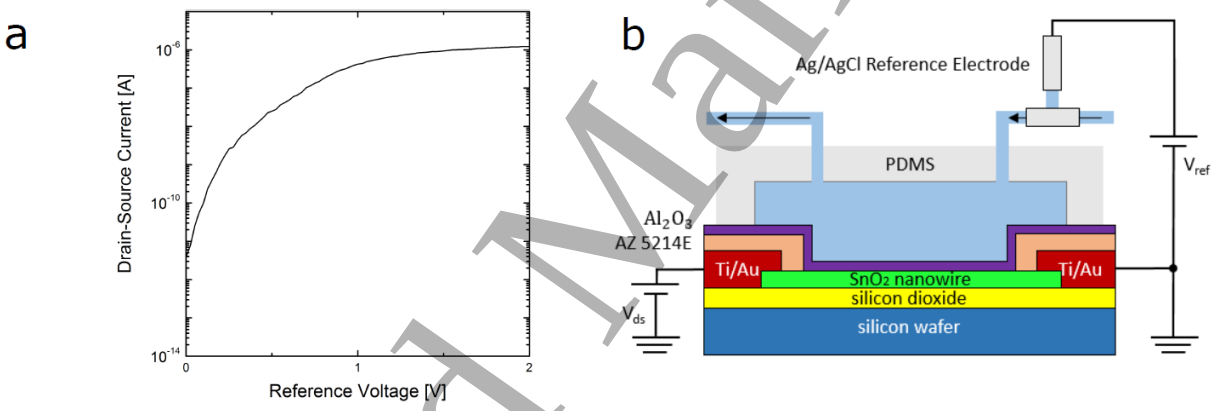

Figure 3. (a) Transfer (semi-logarithmic scale) characteristics (I_{ds} – V_{ref}) of a SnO_2 NW-FET pH sensor with liquid gate potential at V_{ds} = 100 mV. (b) Schematic side view diagram of a SnO_2 NW-FET pH sensor embedded in a microfluidic cell.

Before starting the real-time pH measurement the I_{ds} – V_{ds} output characteristics (drain-source voltage V_{ds} from 0 V to 0.5 V) from a second SnO_2 NW-FET pH sensor for pH ranging from pH 3 to pH 10 were taken at room temperature (no graph shown). It is clearly recognizable that a decrease of the output drain-source current is observed with an increase in pH of the electrolyte solution. For pH 3 the electrolyte solution is extremely acidic with a high amount of

positively charged H^+ ions. In comparison, for pH 10, the amount of negatively charged OH^- ions predominates [34]. The electrolyte solution is very strongly alkaline. The chemical reactions close to the insulator surface can be explained by the site-binding model [40]. If the pH is now increased from pH 3 to pH 4 the amount of positively charged $AlOH_2^+$ groups on the sensor surface which are attracting electrons in the n-type semiconductor channel is decreasing. Accordingly, the number of negatively charged AlO^- groups on the sensor surface is increasing [41]. As a result, the channel is getting less conductive and the drain-source current is decreasing.

After proving in principle the decrease of drain-source current for increasing pH as a next step the real-time measurement $G_{ds} - t$ of eight electrolyte buffer solutions with pH values changing from 3 to 10 is shown. Fig. 4a shows the corresponding linear transfer characteristics by sweeping the reference voltage V_{ref} from -0.4 V to 0.4 V at a constant drain-source voltage V_{ds} = 100 mV of the in the following investigated SnO_2 NW-FET pH sensor. Comparing the inset of Fig. 4a showing the transfer characteristics in semi-logarithmic scale shows a similar drain-source current behavior as already observed for the SnO_2 NW-FET with metal top gate (Fig. 2a Inset). Based on the drain-source current depicted in Fig. 4a, a reference voltage of V_{ref} = 200 mV (I_{ds} = 3.5 10^{-8} A in pH 3) was chosen to be applied during the real-time measurement. A constant reference voltage lower than V ~ 0.4 V (steepest point of linear transfer curve in Fig. 4a) was chosen to keep the electric field within the electrolyte solution as low as possible while still being able to detect a drain-source current change. Starting the real-time measurement, a conductance of G_{ds} = 4.8 10-7 S (≙ I_{ds} = 4.8 10^{-8} A) can be observed. The increase (ΔI_{ds} = 1.3 10^{-8} A) in drain-source current can be led back to the base line drift of the pH sensor [42–45]. Base line drift is an already known challenge in ISFETs, where ions from the electrolyte solution can diffuse into the gate oxide [43]. In Fig. 4b the first significant change in

conductance ($G = I_{ds}/V_{ds}$) can be observed after changing the solution from pH 3 to pH 4. An immediate amplitude in conductance appears. The difference in step height when changing from one electrolyte to the next might be explained by different ionic-strength of the individual solutions. According to Tarasov *et al.*, using solutions with various ionic-strengths higher than 10 mM lead to additional changes of conductance-flow due to competing surface reaction of H^+ ions and salt ions [46]. The change of conductance for different pH values therefore reflects a change of pH itself ***and*** change of ionic concentration. The inset in Fig. 4b shows the extracted conductance from the real-time pH measurements for changing pH values. As it was the case for the investigated $I_{ds} - V_{ds}$ output characteristics an increase in pH (less positive H^+ ions, more negative OH^- ions) goes along with a decrease in conductance. Using a p-type nanowire instead would lead to an increase in conductance when increasing the pH value [46].

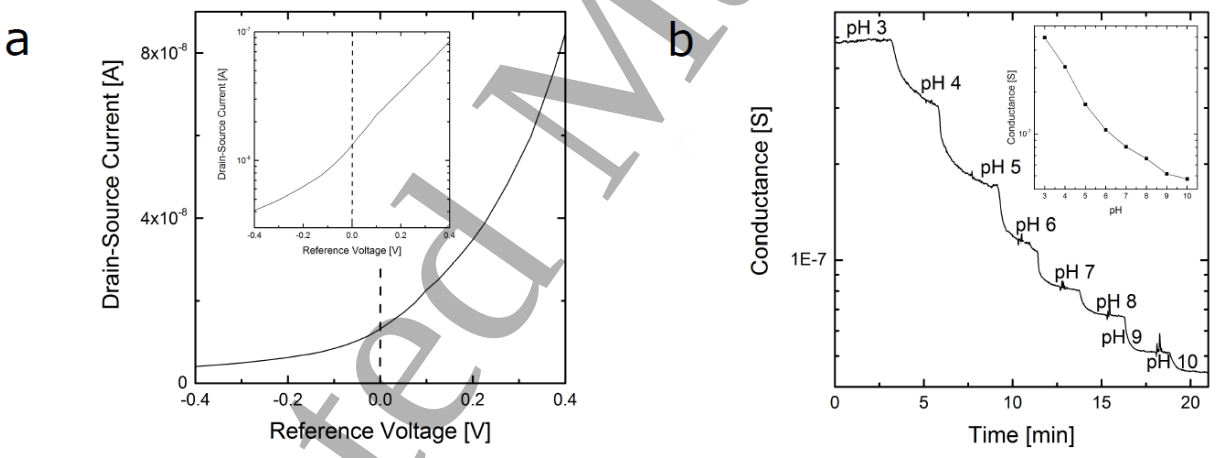

Figure 4. (a) Linear transfer characteristics ($I_{ds} - V_{ref}$) of a SnO_2 NW-FET pH sensor with liquid gate potential at V_{ds} = 100 mV in pH 3. Inset: Transfer characteristics in semi-logarithmic scale (b) Real-time pH measurement ($G_{ds} - t$) showing the change in conductance of the SnO_2 NW-FET pH sensor characterized in Fig. 4a from pH 3 to pH 10 at V_{ref} = 200 mV and V_{ds} = 100 mV. Inset: Conductance of SnO_2 NW-FET pH sensor exposed from pH 3 to pH 10 extracted from the real-time measurement.

III. Protein Detection

In this section we utilize the above shown SnO_2 NW-FET pH sensor to become a biosensor. This was done by an additional functionalization procedure of the active nanowire sensor surface. The measurement setup stays unchanged as seen in Fig. 3b. The protein streptavidin, chosen for its strong binding affinity to biotin, was employed as bio-receptor to show the successful detection of a biotinylated protein (here the tetracycline repressor TetR) using our SnO_2 NW-FET biosensor.

The field-effect transistor can be used as a charge detector when the respective biomolecules are sufficiently close to the sensor surface. Under physiological conditions most proteins carry an intrinsic negative or positive charge. The charge of the biomolecule directly depends on its isoelectric point (pI) and on the pH value of the electrolyte solution in which it is diluted. If the pI of a protein is higher than the pH of the dilution buffer, the protein will be positively charged. In contrast, if the pI of the protein is lower than the pH of the dilution buffer, it will be negatively charged [47]. The PBS buffers employed in this work have a pH ranging from 7.4 (0.01 × PBS) to 7.8 (1 × PBS). Therefore streptavidin (pI: 5 [48]), BSA (pI: 4.7 [49]) and TetR (pI: 6.0 [50]) should be negatively charged in all PBS solutions used here. As a result, when the target molecule bTetR comes in close contact to the functionalized sensor it is drawn to the sensor surface and specifically and almost irreversibly binds to its receptor molecule streptavidin [12]. This ideally results in a drain-source current change in the nanowire. However, electrically detecting biomolecules using charge detection by the field-effect in electrolyte solutions is strongly limited by the Debye screening length. The latter is mainly determined by the salt concentration of the electrolyte. Mobile ions efficiently screen the charges of the biomolecules at physiological salt concentrations. As a result only a small or no change of current might be

detected [51]. While the successful measurements of proteins in 0.01 M PBS (1 × PBS) have been shown [52], it is widely accepted that generally lower salt concentrations compared to physiological conditions become necessary [53]. The Debye screening length is given by $\lambda_D = (\varepsilon_r \varepsilon_0 k_B T / q^2 I)^{1/2}$, where ε_r is the dielectric constant, ε_0 is the permittivity of free space, k_B is the Boltzmann constant, T is the absolute temperature in Kelvin, q is the elemental charge and I the ionic strength of the electrolyte solution [51]. When diluting PBS to 0.1 × PBS, the Debye length can be increased from 0.7 nm to 2.3 nm (Fig. 5b). Even further dilution down to 0.01 × PBS increases the Debye length to 7.3 nm [54]. This means that bigger parts of the biomolecules are within the detection range of the nanowire as can be seen in Fig. 5b. Using only receptor fragments which allows the target molecule to be closer to the sensor surface is another approach to bypass a short Debye length in high salt concentrations [53]. The main challenge for protein detection with the NW-FET technology is therefore to find appropriate assay conditions which enable the measurement of an electric charge within the Debye screening length while maintaining adequate buffer conditions (e. g. pH, salt concentrations) compatible with protein stability and functionality. Keeping these criteria in mind, several buffers with different ionic strength were tested for the detection of our biotinylated protein. In addition, and as a first step the ELISA technique was used to attest of the functionality of the bioassay in different buffer conditions. Once appropriate conditions were established the assay was transferred to the NW-FET for the electrical detection of protein.

ELISA Measurement

To determine the optimal measurement procedure for protein detection different ELISA protocols were tested. As a first step binding capacity in a high ionic-strength (1 × PBS) and a low ionic-strength (0.1 × PBS) solution using ELISA was explored. Fig. 5a shows an increasing signal with increasing bTetR concentration from 0 ng/ml to 60,000 ng/ml in undiluted (1 ×)

PBS. However, for diluted (0.1 x) PBS no increase in signal can be detected. Changing the ionic-strengths seems to have a direct influence on the stability of the proteins or on the binding affinity between streptavidin and biotin. We suggest that with a decreasing salt concentration proteins lose parts of their binding properties. To bypass this challenge, while at the same time allowing to electrically measure a signal, two more measurement procedures were tested. Hereby we decided to conduct all protein related steps such as BSA surface passivation and specific binding in undiluted (1 ×) PBS. However, the washing steps in between were performed with either 0.1 × or 0.01 × PBS. An increase in signal can be seen for an increase in bTetR concentration (Fig. 5a). When comparing it to the first ELISA procedure conducted solely in 1 × PBS it can be seen that washing away unbound proteins becomes more difficult the more diluted the washing buffer is. For future measurements we therefore recommend to start washing the microfluidic cell with 1 × PBS followed by a second washing step with 0.01 × PBS allowing for a screening reduction and therefore potentiometric electrical measurements.

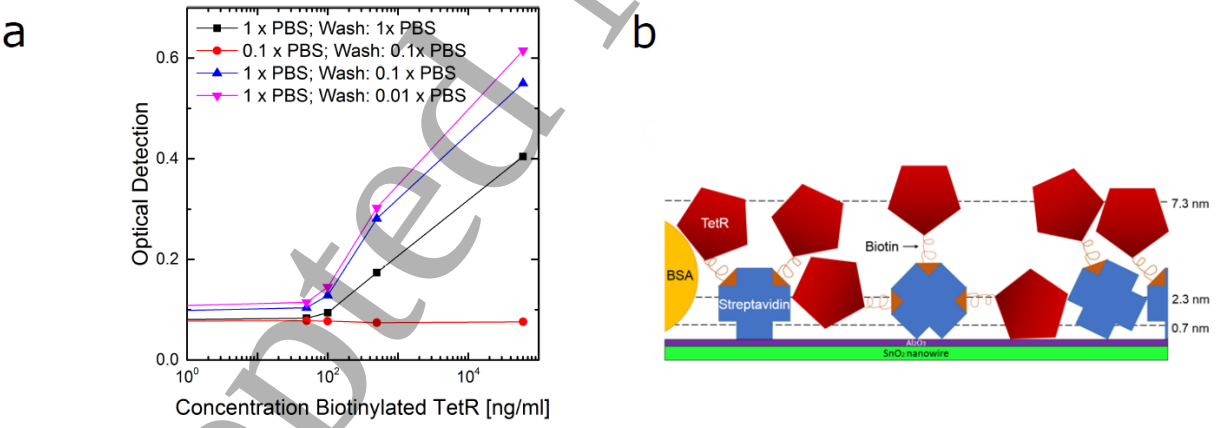

Figure 5. (a) Detection of bTetR based on Enzyme-Linked Immunosorbent Assay (ELISA). ELISA of bTetR in undiluted (1 × PBS; Wash: 1 × PBS) and diluted (0.1 × PBS; Wash: 0.1 × PBS) PBS environment and with washing steps being carried out with 0.1 × PBS (1 × PBS; Wash: 0.1 × PBS) and 0.01 × PBS (1 × PBS; Wash: 0.01 × PBS). Absorbance was measured at 405 nm. (b) Specific protein binding schematic (not to scale) between bTetR and Streptavidin.

The plotted Debye lengths shows the charge screening for different ionic-strengths solutions (1 × PBS: 0.7 nm; 0.1 × PBS: 2.3 nm; 0.01 × PBS: 7.3 nm).

SnO_2 NW-FET Biosensor

Before starting the bio-functionalization process the quality of the used SnO_2 NW-FET biosensor was tested. For this the $I_{ds} - V_{ds}$ curve was measured at a drain-source voltage of V_{ds} = 100 mV using a reference voltage from 0 V to 0.5 V. A good ohmic behavior between the SnO_2 nanowire and Ti/Au contacts was extracted. To be able to see the successive influence of the proteins on the sensor surface the transfer characteristics is measured after each protein step. Fig. 6 shows the collected transfer characteristics $I_{ds} - V_{ref}$ of the SnO_2 NW-FET biosensor at room temperature after streptavidin functionalization, BSA surface passivation and bTetR injection. The applied constant drain-source voltage is set to V_{ds} = 100 mV. The liquid gate is swept from -0.5 V to 0.5 V. It can be seen that the drain-source current of the SnO_2 NW-FET biosensor can be modulated from $I_{ds} < 10^{-12}$ A to $I_{ds} \sim 10^{-8}$ A for reference voltages from 0 V to 0.5 V, respectively. To compare it to the earlier described pH sensor a drain-source current modulation from $I_{ds} > 10^{-12}$ A to $I_{ds} \sim 10^{-8}$ A for 0 V to 0.5 V reference voltage, respectively, was possible. Please note that two different SnO2 NW-FET pH sensors/biosensors show similar transfer characteristics and thus are a good indication of the reproducibility and reliability of the produced devices.

Binding of charged proteins lead to a positive or negative shift of the transfer curve depending on the protein charge in the electrolyte. However, the incline of the $I_{ds} - V_{ref}$ should stay the same throughout the measurement [25] as seen in the inset of Fig. 6. To quantitatively determine the impact of proteins on the sensor surface the reference voltage shifts are extracted at $I_{ds} = 10^{-}$

^{10} A (Inset Fig. 6). Sensor surface passivation with BSA proteins led to a positive shift of the transfer curve of 17.8 mV compared to the original curve with only streptavidin on the sensor surface. A second positive shift of 23.7 mV can be seen after protein interaction of bTetR and streptavidin. As expected, the positive shifts confirm the existence of both negative charged BSA on the sensor surface and a successful bond between streptavidin and negatively charged bTetR. According to Hagen *et al.* a positive shift of the transfer curve, leading to an increased threshold voltage, can also be interpreted as additional deposition of electrically resistive molecules to the sensor surface [11]. This added layer equates to a thicker gate insulation. As a result, the transfer characteristics is stretched as directly observed (Fig. 6). Therefore, we conclude a successful potentiometric detection of TetR.

While we were able to proof the sensitivity of Al_2O_3-coated SnO_2 NW-FETs to protons as well as to a specific protein, further tests have to be made determine the limit of detection of the here presented sensor. A low limit of detection is especially needed when it comes to early disease diagnostics. Current protein detections methods, such as ELISA, show sensitivities down to the 10 pg/ml range [55]. In contrast, for the here presented proof-of-concept, a concentration of 600 µg/ml was used. Decreasing the concentration of the investigated protein obviously goes along with a decrease in the reference voltage shift. To compensate the overall reduction of the investigated protein within the electrolyte solution, one possibility is to only functionalize the nanowire with the receptor molecule instead of the whole inner device surface which is not being used for sensing [27]. For silicon nanowire FETs, the detection of 100 fM was already proven to be possible [56].

Our potentiometric sensor appears as an attractive alternative to standard ELISA techniques. First of all, given the very small size of the sensor, only a limited sample volume is required.

This is of particular interest in prospect of healthcare applications where certain types of samples are precious and very limited. Secondly, the label free detection of the presented sensor enables a rapid measurement, considerably facilitating and accelerating the assay procedure. While a real-time measurement was shown for changing pH, doing so for the here investigated bTetR was not possible due to the loss of the binding characteristics of bTetR to streptavidin in diluted PBS (Fig. 5). At the same time, at higher electrolyte concentrations, all charges are screened because of the small Debye length. For real-time measurements it is not possible to go around this challenge by introducing a washing step with a diluted electrolyte solution as it was done for the transfer curves (Fig. 6). However, we do believe that real-time protein detection is, in principle, possible with the here presented SnO_2 NW-FET biosensor when choosing a protein binding pair which keeps its binding properties in diluted PBS. Finally the reduced size of our device (2 cm × 2 cm) makes of it an interesting candidate for further development as a portable diagnostic test for direct on-site measurements. At this stage, we were able to detect the presence of a biotinylated protein, using streptavidin as bio-receptor. However we did not further investigate the sensitivity of the sensor nor its responsiveness to different analyte concentrations. The biggest disadvantage of the SnO_2 NW-FET at the current state is the rather time consuming and complex device fabrication. However, we believe that further optimization steps in the fabrication process could lead to cheaper and faster production. Taken together, given the demonstrated initial potential of our sensor, we expect it to become in future a promising solution for the development of POC devices.

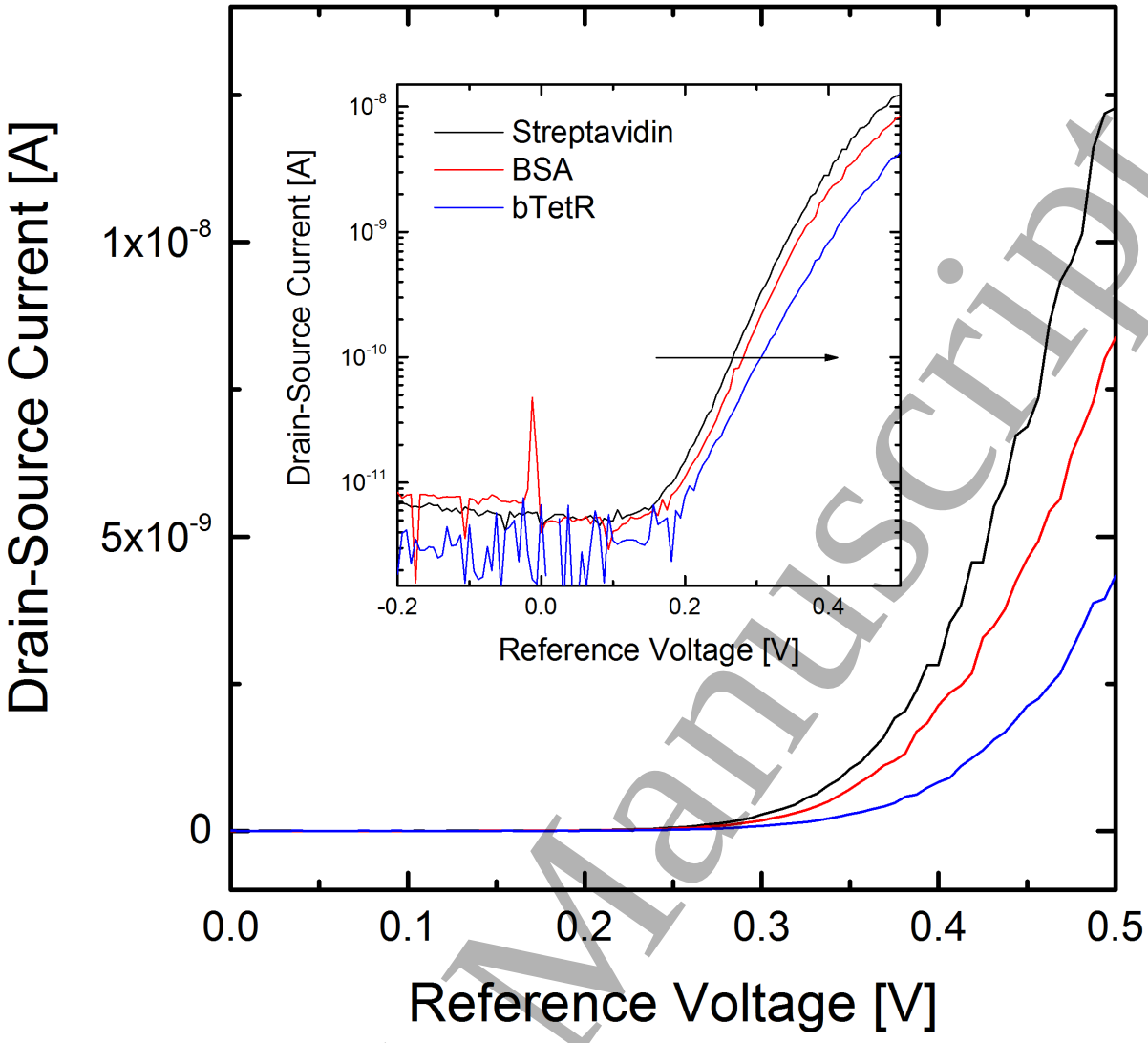

Figure 6. Linear transfer characteristics $I_{ds} - V_{ref}$ of a SnO_2 NW-FET biosensor. Washing steps were done successively in 1 × PBS and 0.01 × PBS. Inset: Semi-logarithmic transfer characteristics $I_{ds} - V_{ref}$. Extraction of the reference voltage at $I_{ds} = 10^{-10}$ A shows a positive shift of 17.8 mV after surface passivation with BSA. After target binding of bTetR to its receptor streptavidin an additional shift of 23.7 mV can be measured.

CONCLUSIONS

In summary, we present a reliable NW-FET sensitive to pH and protein variations requiring only a small volume sample. SnO_2 nanowires grown by VLS are contacted and embedded into a microfluidic measurement setup with a flow-thru Ag/AgCl reference electrode. We successfully show the potentiometric analysis ranging from pH 3 to pH 10. A real-time measurement $G_{ds} - t$ shows the step wise decline of conductance for increasing pH values. For biomolecule detection an ELISA was used to define an optimal measurement procedure for the detection of a biotinylated protein. Screening effects have been minimized by using diluted (0.01 ×) PBS as measurement buffer. For the first time a SnO_2 NW-FET was used to successfully detect a specific protein in an electrolyte solution. Successful detection of bTetR was shown as proof-of-concept for the label-free detection of proteins in low ionic-strength solutions. Streptavidin-biotin as binding pair was used for the detection of bTetR with a high concentration of 600 µg/ml. For further sensor applications we currently investigate the concentration dependency of the SnO_2 NW-FET down to even lower concentrations.

ACKNOWLEDGEMENTS

We gratefully acknowledge financial support from the German Research Foundation (DFG) under contract ZA 191/33-1.

References

[1] K.-I. Chen, B.-R. Li, Y.-T. Chen, Nano Today 6 (2011) 131–154.
[2] M.-Y. Shen, B.-R. Li, Y.-K. Li, Biosensors and Bioelectronics 60 (2014) 101–111.
[3] E. Stern, A. Vacic, M.A. Reed, IEEE Trans. Electron Devices 55 (2008) 3119–3130.
[4] G.-J. Zhang, J.H. Chua, R.-E. Chee, A. Agarwal, S.M. Wong, Biosensors & bioelectronics 24 (2009) 2504–2508.
[5] G.-J. Zhang, L. Zhang, M.J. Huang, Z.H.H. Luo, G.K.I. Tay, E.-J.A. Lim, T.G. Kang, Y. Chen, Sensors and Actuators B: Chemical 146 (2010) 138–144.
[6] F. Patolsky, G. Zheng, O. Hayden, M. Lakadamyali, X. Zhuang, C.M. Lieber (2004) 14017–14022.
[7] W.U. Wang, C. Chen, K.-h. Lin, Y. Fang, C.M. Lieber, Proceedings of the National Academy of Sciences of the United States of America 102 (2005) 3208–3212.
[8] M. Curreli, Rui Zhang, F.N. Ishikawa, Hsiao-Kang Chang, R.J. Cote, Chongwu Zhou, M.E. Thompson, IEEE Trans. Nanotechnology 7 (2008) 651–667.
[9] J. Liu, J. Goud, P.M. Raj, M. Iyer, Z. Wang, R.R. Tummala (2007) 1971–1976.
[10] A. Choi, K. Kim, H.-I. Jung, S.Y. Lee, Sensors and Actuators B: Chemical 148 (2010) 577–582.
[11] J.A. Hagen, S.N. Kim, B. Bayraktaroglu, K. Leedy, J.L. Chávez, N. Kelley-Loughnane, R.R. Naik, M.O. Stone, Sensors (Basel, Switzerland) 11 (2011) 6645–6655.
[12] J. Liu, J. Goud, P.M. Raj, M. Iyer, Z.L. Wang, R.R. Tummala (2008) 1317–1322.
[13] S.M. Sultan, K. Sun, de Planque, Maurits R. R., P. Ashburn, H.M.H. Chong, Top-Down Fabricated ZnO Nanowire Transistors for Application in Biosensors, IEEE, Piscataway, NJ, 2012.
[14] Y.-J. Choi, I.-S. Hwang, J.-G. Park, K.J. Choi, J.-H. Park, J.-H. Lee, Nanotechnology 19 (2008) 95508.
[15] A. Kolmakov, Y. Zhang, G. Cheng, M. Moskovits, Adv. Mater. 15 (2003) 997–1000.
[16] M.T. Björk, H. Schmid, J. Knoch, H. Riel, W. Riess, Nature nanotechnology 4 (2009) 103–107.
[17] Q. Kuang, C. Lao, Z.L. Wang, Z. Xie, L. Zheng, Journal of the American Chemical Society 129 (2007) 6070–6071.
[18] R. Yu, J. Yun, Y. Kim, Archives of Metallurgy and Materials 60 (2015).
[19] R.A. Rani, O. Sidek, IEEE (2004) 660–663.
[20] J. Go, P.R. Nair, B. Reddy, B.R. Dorvel, R. Bashir, M.A. Alam, IEEE (2010).
[21] K. Bedner, V.A. Guzenko, A. Tarasov, M. Wipf, R.L. Stoop, D. Just, S. Rigante, W. Fu, Minamisawa R. A., C. David, M. Calame, J. Gobrecht, C. Schönenberger, Sensors and Materials 25 (2013) 567–576.
[22] P. Bergveld, Biosensors 2 (1986) 15–33.
[23] Luc Bousse, Nico F. De Rooij, Piet Bergveld, IEEE Trans. Electron Devices (1983).
[24] Y. Wang, G. Li (2010).
[25] X. Duan, Y. Li, N.K. Rajan, D.A. Routenberg, Y. Modis, M.A. Reed, Nature nanotechnology 7 (2012) 401–407.
[26] B. Khamaisi, O. Vaknin, O. Shaya, N. Ashkenasy, ACS nano 4 (2010) 4601–4608.
[27] B.-R. Li, C.-W. Chen, W.-L. Yang, T.-Y. Lin, C.-Y. Pan, Y.-T. Chen, Biosensors & bioelectronics 45 (2013) 252–259.
[28] J.-H. Ahn, J.-Y. Kim, K. Choi, D.-I. Moon, C.-H. Kim, M.-L. Seol, T.J. Park, S.Y. Lee, Y.-K. Choi, IEEE Trans. Electron Devices 59 (2012) 2243–2249.
[29] D. Tsivion, M. Schvartzman, R. Popovitz-Biro, P. von Huth, E. Joselevich, Science (New York, N.Y.) 333 (2011) 1003–1007.
[30] D. Tsivion, M. Schvartzman, R. Popovitz-Biro, E. Joselevich, ACS nano 6 (2012) 6433–6445.
[31] M.W. Shinwari, D. Zhitomirsky, I.A. Deen, P.R. Selvaganapathy, M.J. Deen, D. Landheer, Sensors (Basel, Switzerland) 10 (2010) 1679–1715.

[32] K. Besteman, J.-O. Lee, F.G.M. Wiertz, H.A. Heering, C. Dekker, Nano Lett. 3 (2003) 727–730.
[33] E.D. Minot, A.M. Janssens, I. Heller, Applied physics letters 91 (2007) 93507.
[34] A. Menzel, Large-Scale Functional Nanostructures and Nanodevices, 2013.
[35] A. Menzel, K. Subannajui, F. Güder, D. Moser, O. Paul, M. Zacharias, Adv. Funct. Mater. 21 (2011) 4342–4348.
[36] A. Tarasov, D.W. Gray, M.-Y. Tsai, N. Shields, A. Montrose, N. Creedon, P. Lovera, A. O'Riordan, M.H. Mooney, E.M. Vogel, Biosensors & bioelectronics 79 (2016) 669–678.
[37] E.N. Dattoli, Q. Wan, W. Guo, Y. Chen, X. Pan, W. Lu, Nano letters 7 (2007) 2463–2469.
[38] M.S. Arnold, P. Avouris, Z.W. Pan, Z.L. Wang, J. Phys. Chem. B 107 (2003) 659–663.
[39] N.H. Van, J.-H. Lee, J.I. Sohn, S.N. Cha, D. Whang, J.M. Kim, D.J. Kang, Nanoscale 6 (2014) 5479–5483.
[40] L.K. Meixner, S. Koch, Sensors and Actuators B: Chemical 6 (1992) 315–318.
[41] M.-P. Lu, C.-Y. Hsiao, W.-T. Lai, Y.-S. Yang, Nanotechnology 21 (2010) 425505.
[42] Y. Ito, Sensors and Actuators B: Chemical 66 (2000) 53–55.
[43] S. Jamasb, S. Collins, R.L. Smith, Sensors and Actuators B: Chemical 49 (1998) 146–155.
[44] J.-J. Xu, X.-L. Luo, H.-Y. Chen, Frontiers in bioscience a journal and virtual library 10 (2005) 420–430.
[45] D. Pijanowska, W. Torbicz, Optoelectronic and Electronic Sensors 210 (1995).
[46] A. Tarasov, M. Wipf, R.L. Stoop, K. Bedner, W. Fu, V.A. Guzenko, O. Knopfmacher, M. Calame, C. Schönenberger, ACS nano 6 (2012) 9291–9298.
[47] P.R. Nair, M.A. Alam, IEEE Trans. Electron Devices 54 (2007) 3400–3408.
[48] J.H. Choi, K.H. Chen, M.S. Strano, Journal of the American Chemical Society 128 (2006) 15584–15585.
[49] Z.G. Peng, K. Hidajat, M.S. Uddin, Journal of colloid and interface science 271 (2004) 277–283.
[50] A. Mortlock, Nucleic Acids Research 31 (2003) 152e-152.
[51] G.S. Kulkarni, Z. Zhong, Nano letters 12 (2012) 719–723.
[52] J.S. Kim, W.I. Park, C.-H. Lee, G.-C. Yi, Journal of the Korean Physical Society (2006).
[53] R. Elnathan, M. Kwiat, A. Pevzner, Y. Engel, L. Burstein, A. Khatchtourints, A. Lichtenstein, R. Kantaev, F. Patolsky, Nano letters 12 (2012) 5245–5254.
[54] J.H. Chua, R.-E. Chee, A. Agarwal, S.M. Wong, G.-J. Zhang, Analytical chemistry 81 (2009) 6266–6271.
[55] G.-J. Zhang, Y. Ning, Analytica Chimica Acta 749 (2012) 1–15.
[56] E. Stern, J.F. Klemic, D.A. Routenberg, P.N. Wyrembak, D.B. Turner-Evans, A.D. Hamilton, D.A. LaVan, T.M. Fahmy, M.A. Reed, Nature 445 (2007) 519–522.